Bidirectional transendothelial migration of monocytes across hepatic sinusoidal endothelium shapes monocyte differentiation and regulates the balance between immunity and tolerance in liver

Zimmermann, Henning W; Bruns, Tony; Weston, Chris J; Curbishley, Stuart M; Liaskou, Evaggelia; Li, Ka-Kit; Resheq, Yazid J; Badenhorst, Paul W; Adams, David H

DOI:
10.1002/hep.28285

BIDIRECTIONAL TRANSENDOTHELIAL MIGRATION OF MONOCYTES ACROSS HEPATIC SINUSOIDAL ENDOTHELIUM SHAPES MONOCYTE DIFFERENTIATION AND REGULATES THE BALANCE BETWEEN IMMUNITY AND TOLERANCE IN LIVER

Short title: Migration across HSEC and monocyte function

Authors:

1. Henning W Zimmermann (1,2) henzimmermann@ukaachen.de
2. Tony Bruns (1,3,4) tony.bruns@med.uni-jena.de
3. Chris J Weston (1) c.j.weston@bham.ac.uk
4. Stuart M Curbishley (1) s.m.curbishley@bham.ac.uk
5. Evaggelia Liaskou (1) e.liaskou@bham.ac.uk
6. Ka-Kit Li (1) kkl5@doctors.org.uk
7. Yazid J Resheq (1,5) Yazid.Resheq@uk-erlangen.de
8. Paul W. Badenhorst (6) p.w.badenhorst@bham.ac.uk
9. David H Adams (1) d.h.adams@bham.ac.uk

Affiliations:

1. NIHR Biomedical Research Unit and Centre for Liver Research, University of Birmingham, Birmingham, United Kingdom

2. Department of Medicine III, University Hospital Aachen, RWTH Aachen University, Aachen, Germany

3. Department of Internal Medicine IV, Jena University Hospital, Friedrich Schiller University of Jena, Jena, Germany

4. Center for Sepsis Control and Care, Jena University Hospital, Friedrich Schiller University of Jena, Jena, Germany

5. Department of Internal Medicine 5, Hematology and Oncology, University of Erlangen-Nuremberg, Erlangen, Germany

6. School of Immunity and Infection, University of Birmingham, Birmingham, UK

This article has been accepted for publication and undergone full peer review but has not been through the copyediting, typesetting, pagination and proofreading process which may lead to differences between this version and the Version of Record. Please cite this article as doi: 10.1002/hep.28285

Corresponding authors:

1. David H. Adams, MD, FRCP, FMedSci, Centre for Liver Research, 5th Floor IBR, College of Medical and Dental Sciences, Medical School Building, University of Birmingham, Edgbaston, Birmingham, B15 2TT, UK. Telephone +44 (0)121 415 8702. Email: d.h.adams@bham.ac.uk
2. Henning Zimmermann, MD, Department of Medicine III, University Hospital of Aachen, Pauwelsstr. 30, 52072 Aachen, Germany. Telephone +49 241 80 36226. Email: henzimmermann@ukaachen.de

Grant Support:

Henning W Zimmermann was supported by the START-program of the medical faculty of the University of Aachen / Germany with additional funding from a Wellcome Trust Programme award held by David H Adams.

Disclosures:

The authors have nothing to disclose.

Author Contributions:

Study concept and design: HWZ, DHA
Acquisition of data: HWZ, TB, PWB
Analysis and interpretation of data: HWZ, CJW, DHA
Drafting of the manuscript: HWZ, DHA
Critical revision of the manuscript for important intellectual content: HWZ, TB, CJW, SMC, EL, KL, YJR, PWB, DHA
Statistical analysis: HWZ, PWB
Technical and material support: TB, CJW, SMC, EL, KL, YJR, PWB, DHA
Study Supervision: DHA

Abstract: (239 words)

Background: Monocytes are versatile cells that can fulfil pro- and anti-inflammatory functions when recruited to the liver. Recruited monocytes differentiate into tissue macrophages and dendritic cells, which sample antigens and migrate to lymph nodes to elicit T-cell responses. The signals that determine monocyte differentiation and the role of hepatic sinusoidal endothelial cells (HSEC) in this process are poorly understood. HSEC are known to modulate T-cell activation leading us to investigate whether transendothelial migration (TEM) of monocytes across HSEC influences their phenotype and function. **Materials and Methods:** Subsets of blood-derived monocytes were allowed to transmigrate across human HSEC into a collagen matrix. Most migrated cells remained in the subendothelial matrix but ~10% underwent spontaneous basal to apical TEM. The maturation, cytokine secretion and T-cell stimulatory capacity of reverse transmigrating (RT) and subendothelial (SE) monocytes were compared. **Results:** SE-monocytes were mainly CD16$^-$ whereas 75–80% of RT-monocytes were CD16$^+$. SE-monocytes derived from the CD14++CD16− subset and exhibited high phagocytic activity whereas RT-monocytes originated from CD14++CD16+ and CD14+CD16++ monocytes, displayed an immature DC-like phenotype (CD11c^{pos}HLA-DR^{pos}CD80$_{lo}$CD86$_{lo}$) and expressed higher levels of CCR8. Consistent with a DC-phenotype RT-monocytes secreted inflammatory cytokines and induced Ag-specific CD4+ T-cell activation. In contrast, SE-monocytes suppressed T-cell proliferation and activation and exhibited endotoxin tolerance. Transcriptome analysis underscored the functional differences between SE and RT-monocytes. **Conclusions:** Migration across HSEC shapes the subsequent fate of monocytes giving rise to anergic macrophage-like cells in tissue and the release of immunocompetent pre-DCs into the circulation.

Key words: liver; immunotolerance; sinusoids; macrophages

Introduction:

Monocytes fulfil important functions in the defense against pathogens by linking innate to adaptive immunity.(1) Their plasticity and inherent heterogeneity allows monocytes to give rise to tissue-resident macrophages and dendritic cells (DC).(2-5) Macrophage precursor cells display phagocytic activity and can clear senescent cells, microbial and other foreign material to promote tissue repair and remodeling. During steady-state conditions monocytes traverse the endothelium to enter tissue from blood in order to replenish and augment the local pool and this process is greatly increased with inflammation.(5) A substantial minority of monocytes with a DC-like phenotype sample antigens in the subendothelial compartment and migrate to afferent lymph nodes.(2) Human monocytes comprise three morphologically and functionally distinct subsets based on expression of CD14 and CD16: 'classical' $CD14^{++}CD16^{-}$; 'intermediate' $CD14^{++}CD16^{+}$ and 'non-classical' $CD14^{+}CD16^{++}$ monocytes.(6, 7)

Monocytes traffic to the liver under normal conditions and this increases markedly in response to liver injury.(8, 9) We previously showed that monocyte subpopulations differentially accumulate in the inflamed liver although the mechanisms that control their recruitment and positioning are poorly understood.(10) Hepatic sinusoidal endothelial cells (HSEC) differ morphologically and functionally from endothelial cells in other vascular beds and actively control the translocation of circulating immune cells from the sinusoids into the liver parenchyma.(11) .(12) Importantly, HSEC modulate local immunity by, for instance, skewing Th1 and Th17 responses to to induce suppressive T-cells thereby contributing to the prevailing immune regulatory hepatic microenvironment.(13, 14) We hypothesized that transendothelial migration across activated HSEC shapes monocyte fate and differentiation thereby regulating hepatic immune responses.

Because monocytes not only migrate from blood into tissue but also undergo reverse transmigration out of tissue into the blood we studied uni- and bidirectional migration of monocyte subsets across human HSEC to determine how these processes affect

subsequent monocyte function. We report that $CD16^+$ monocytes preferentially undergo reverse transmigration after which they can activate $CD4^+$ T-cells whereas monocytes that remain in the subendothelial space resemble anti-inflammatory macrophages that promote T-cell anergy. Functional differences following transendothelial migration are accompanied by substantial changes in the transcriptome. Thus TEM across endothelium contributes to hepatic immune regulation.

Materials and Methods

Isolation and culture of endothelial cells:

HSEC were isolated from human explanted or resected liver and surplus donor tissue as previously described.(15) Briefly, parenchymal cells were isolated from collagenase-digested tissue over a 33/77% Percoll gradient (Amersham Biosciences, GE Healthcare, Little Chalfont, U.K.) and magnetic selection with antibody HEA125 (Progen Biotechnik, Germany) used to deplete cholangiocytes followed by anti-CD31 selection of HSEC (Invitrogen, Paisley, U.K.) and culture in human endothelial basal growth medium (EBM, Invitrogen), 10% (v/v) heat-inactivated AB human serum (HD Supplies, Glasgow, U.K.), 10 ng/ml vascular endothelial growth factor (VEGF), and 10 ng/ml hepatocyte growth factor (HGF) (PeproTech, Peterborough, U.K.) in collagen-coated culture flasks. All human tissue and blood was collected with local research ethics committee approval and patient consent.

Bidirectional monocyte transmigration across HSEC

Bovine collagen I (Gibco, Life Technologies) 3 mg/ml in 10× MEM medium (Life Technologies) pH 7.4 was polymerized in 24-well cell culture standing inserts (pore size 0.4 µm) at 37°C (Merck Millipore, Watford, UK) equilibrated in supplemented HSEC medium for at least 3 days. To study phagocytosis collagen matrix was supplemented with $1x10^7$ unopsonized fluorescence-labelled Zymosan A BioParticles (Molecular Probes, Invitrogen). Collagen gels were coated with 100µl fibronectin at 37°C for 30 min (Invitrogen/Gibco; 50 µg/ml in PBS) and seeded with HSEC grown until confluence following stimulation with 10 ng/ml TNFα (Peprotech, UK) and 10 ng/ml /IFN-γ (Peptrotech, UK) for 24h. $2×10^6$ $CD14^+$ monocytes or presorted monocyte subsets in EBM/0.1% BSA were layered onto the fibronectin-coated collagen plugs. After 1.5 hours non-adherent cells were washed off and the media replaced by EBM containing 2.5 % (v/v) heat-inactivated human serum. During the subsequent 48h incubation spontaneously reverse transmigrating (RT) monocytes were harvested by thoroughly washing off cells from above the endothelial layer with ice-cold PBS/ 0.5 mM EGTA/ 1% FCS. The collagen plugs containing retained subendothelial (SE)

monocytes were gently digested in 20% (v/v) collagenase from *Clostridium histolyticum* (Sigma Aldrich,) and 20% (v/v) heat-inactivated FCS at 37°C for 10 minutes. Digests were placed on ice, filtered, and resuspended in PBS/2 mM EDTA/ 1% FCS. We confirmed that surface markers were not lost during collagenase digestion (data not shown). Contaminating HSEC were depleted with biotinylated Ulex Europaeus Agglutinin I (Vector Laboratories, Burlingame, CA) and streptavidin-conjugated Dynabeads© (Life Technologies, Carlsbad, CA) and magnetic depletion. In some experiments HUVEC were used as endothelial cells. RT and SE-monocytes were counted and subjected to further analysis or *in vitro* experiments. Trypan Blue exclusion confirmed viability.

Statistical analysis

Student t test and GraphPad Prism software was used to compare numerical variables between two groups and one-way analysis of variance followed by Bonferroni's post-test for comparisons between more than two groups. Results are expressed as mean ± standard error of the mean. P <0.05 was considered statistically significant. * P<0.05, ** P<0.01, *** P<0.001

For further information on materials and methods please refer to supporting data provided with the full version of the manuscript

Results

Intrahepatic accumulation of monocytes/macrophages is driven by activated endothelial cells

In order to study the fate of monocytes after transmigration to the subendothelial compartment we established a model of monocyte transmigration and reverse transmigration

involving primary human HSEC, adapted from Randolph *et al*.(17) Monocytes were allowed to migrate across activated HSEC and a thin layer of fibronectin into a 3D collagen scaffold. After depletion of non-migrating cells and 2 days of continued co-culture, resident monocytes from the subendothelial compartment (SE-monocytes) and monocytes that underwent spontaneous reverse transmigration (RT-monocytes) from the subendothelial compartment back through the endothelial layer were harvested. To verify that RT-monocytes had sampled the subendothelial compartment, and had not simply detached from the endothelial monolayer, we supplemented the collagen scaffold with FITC-labeled zymosan particles and tracked the localization of phagocytic monocytes/macrophages. Migration into zymosan-supplemented collagen increased the number of retained subendothelial cells most of which were $CD16^{low}$. The RT-monocytes contained zymosan albeit at lower levels than the SE-monocytes and were predominantly $CD16^{high}$ (**Figure 1B**). Long-time imaging could visualize forward and reverse transmigration of monocytes across HSEC under cell-culture conditions (**supplementary video**). In order to confirm that the TEM was an active process we reduced migration in both directions by inhibiting JAK-STAT signaling, which is required for macrophage TEM (18) (**Supplementary Figure S1**). Interestingly, direct comparison of cell compartimentalization after monocyte TEM across HSEC or HUVEC revealed, that HSEC clearly favor subendothelial retention (90% SE-monocytes), whereas HUVEC permitted approximately 50% of monocytes to reverse transmigrate (**Figure 1C**). To mimic the inflammatory environment present in the subendothelial compartment during liver disease, the collagen matrix was supplemented with conditioned medium of activated primary liver myofibroblasts (aLMF). TNFα/IFNγ-stimulation of aLMF led to a profound increase the total number of transmigrating cells though the ratio of RT/SE was not significantly altered **(Supplementary Figure S2)**. These data demonstrate that after active recruitment across HSEC monocytes differentiate into either sessile macrophage-like cells with high phagocytic capacity or mobile dendritic-like cells. Recruitment is augmented by cell-derived chemotactic stimuli.

Reverse transmigrating monocytes express CD16 and can be derived from all monocyte subsets

The majority of SE (mean 78.9% ± 9.8%) monocytes were 'classical' $CD14^{++}CD16^{-}$ monocytes whereas 69.4% (± 12.6%) of RT-monocytes were 'intermediate' $CD14^{++}CD16^{+}$ and few were 'classical' monocytes. Very few cells in either compartment were non-classical $CD14^{+}CD16^{++}$ cells suggesting that this subset does not readily undergo TEM (**Figure 2A**). Monocytes are highly plastic cells and different subsets represent various states of maturity and differentiation prompting us to determine how the different subsets in blood contributed to either SE or RT-monocytes. When classical monocytes were used as the starting cell type >80% were retained in the SE compartment (80.7% ± 12.6) and fewer cells underwent reverse TEM compared with either intermediate and non-classical subsets (**Figure 2B,C**) suggesting that CD16 expression is associated with the ability to undergo RT. Most RT-monocytes were CD16+ indicating that these cells gain CD16 expression either during TEM or in the subendothelial space and that this confers on some cells the ability to undergo reverse transendothelial migration (**Figure 2C**).

Reverse transmigration of monocytes across HSEC imparts a phenotype consistent with immature dendritic cells

We analyzed the different subsets for features of DC differentiation to see if reverse transmigration selects monocytes with the capability to become DC and to re-enter the vasculature before being recruited to lymph nodes through high endothelial venules.(17) Both RT and SE-monocytes expressed high levels of MHC Class II and CD40 (**Figure 3**). CD86 (B7-2) was expressed at higher levels on SE with little CD80 (B7-1) or CD83 detected on either subset. RT-monocytes expressed higher levels of two scavenger receptors: the mannose receptor (CD206) and CD163, both of which are associated with alternatively activated macrophages while CD206 is also present on immature DCs. Neither RT nor SE cells expressed high levels of DC-SIGN (CD209). The classical macrophage marker CD68

was expressed at similar levels on both SE and RT-monocytes. CD11b (Mac-1) and CD11c are integrin alpha chains that form heterodimers with CD18 and bind complement and ICAM-1. CD11c expression is characteristic of DCs and was detected at high levels on RT-monocytes. CCR7 and CCR8 regulate homing of DC to the afferent lymph node.(19) CCR8 was expressed at higher levels on RT-monocytes suggesting that CCR8 might be involved in reverse transmigration. There were no detectable differences in expression of CCR7 or CCR5 on RT versus SE cells and neither subset expressed CCR2 (data not shown). RT-monocytes tended to express higher levels of CX3CR1 and macrophage-colony-stimulating factor receptor (CD115) both of which are characteristic of DC.(20) Thus SE and RT cells are similar in terms of co-stimulatory molecule expression although the RT-monocytes have characteristics of promigratory, DC-like cells.

RT but not SE-monocytes induce robust T-cell proliferation

We compared RT monocyte with SE cells for their ability to induce $CD4^+$ T-cell proliferation, a defining feature of DCs. While SE-monocytes had little effect on T-cell proliferation RT-monocytes induced potent proliferative responses after pulsing with pp65 (**Figure 4A**). We saw a similar although weaker effect in an allogeneic T-cell response (**Figure 4B**). Thus DC-like function resides in the RT population. In the presence of SE-monocytes T-cell proliferation in response to either OKT3 or CD3/CD28 stimulation was significantly suppressed at T-cell ratio/monocyte ratios of 1:1 and below, whereas RT-monocytes amplified baseline proliferation of $CD4^+$ T-cells (**Figure 4C**). The inhibitory effect of SE-monocytes was not due to the induction of apoptosis in CD4+ T-cells (**Figure 4D**).

RT-monocytes are capable of inducing $CD4^+$ T-cell activation whereas SE macrophage-like monocytes dampen activation

Having observed that RT but not SE-monocytes can induce antigen-specific $CD4^+$ T-cell proliferation we next compared the ability of SE and RT-monocytes to drive T-cell activation

using $CD14^+$ monocytes from CMV-seropositive donors (**Figure 5A**). RT-monocytes activated $CD4^+$ T-cells as demonstrated by upregulation of the late-activation markers CD25 and HLA-DR whereas SE-monocytes had no effect on activation and suppressed expression of the mid-early T-cell activation marker CD71 (**Figure 5B,C**). We observed similar effects in an allogeneic system (data not shown). To obtain insights into the consequences of T-cell activation by RT-monocytes we quantified changes in genes involved in T-cell differentiation. SE-monocytes increased expression of *NFATC2* (*NFAT1*), which is linked to CD4+ T-cell anergy and suppression along with Fas ligand (*FASLG*) that triggers activation-induced T-cell apoptosis.(21-23) In contradistinction CD4+ T-cells activated by RT-monocytes expressed T-box transcription factor *EOMES (Eomesodermin)* and *TNFRSF9 (CD137)* (5-fold and 4.76-fold increase, respectively compared with cells stimulated with SE monocyte) (**Figure 5D**). These genes are associated with T cell memory and effector function and promote clonal expansion and T cell survival.[21,22] Cells co-incubated with RT-monocytes also increased expression of several genes that drive Th2 commitment, including *IL13, IRF4*, *GFI1*, *IL4R* and *IL13RA1 (***Figure 5D**) whereas genes that counteract Th2 polarization (*POU2F2* and *RUNX1)* were more highly expressed in T-cells co-cultivated with SE-monocytes.

Reverse transmigrating monocytes induce effector T-cells with Th1-like features

To further characterize the $CD4^+$ T-cell antigen-specific response driven by RT-monocytes we assessed the release of cytokines by activated T cells upon co-culture with CMV pp65 exposed autologous RT/SE-monocytes. RT-monocytes induced a significantly higher proportion of IFN-γ producing T-cells than SE-monocytes suggesting Th1 polarization (**Figure 6A**) although responding $CD4^+$ T-cells also increased CTLA-4 and FOXP3 expression, genes that are linked to regulatory T-cells but also upregulated during early T cell activation. In line with proliferation assays described above, we suggest that RT-monocytes induce activated effector $CD4^+$ T-cells rather than a suppressive phenotype (**Figure 6B,C)**. Despite a genetic profile compatible with Th2 commitment we failed to detect

IL-4 in $CD4^+$ T-cells stimulated with RT-monocytes (**Figure 6C**). Consistent with local IFN-γ secretion the RT-monocytes in the co-cultures showed significantly increased levels of programmed death-ligand 1 (which is strongly induced by interferons) compared with SE-monocytes (**Figure 6D**), whereas its cognate ligand PD-1 was not regulated on co-cultivated $CD4^+$ T-cells (**Figure 6E).** Comparing HSEC- and HUVEC-shaped monocytes we observed that SE-monocytes derived from HUVEC-interaction were able to elicit IFN-γ-secretion by autologous $CD4^+$ T-cells indicating that failure to induce trans Th1 response is a unique feature of liver-specific endothelium **(Figure 6F)**. We conclude that RT-monocytes effectively activate $CD4^+$ T-cells and potentially prime T-helper cell function whereas SE-monocytes suppress T cell activation and blunt their differentiation.

Resident subendothelial monocytes fail to mount a pro-inflammatory response upon TLR engagement

Having shown differences in the ability of SE and RT-monocytes to induce T cell activation, we compared their ability to respond to TLR engagement. Under baseline conditions after 24h *in vitro* culture, RT and SE-monocytes secreted low levels of macrophage migration inhibitory factor (MIF), IL-8 and the anti-inflammatory IL-1RA. SE-monocytes also secreted the chemokines CXCL1, CCL2 and CCL5. Neither RT nor SE-monocytes spontaneously secreted the pro-inflammatory cytokines IL-1β, TNF-α or IL-6 (**Figure 7A,B**). Upon LPS stimulation both subsets secreted IL-6 showing the potential to respond to TLR-4 engagement but while RT-monocytes showed a pro-inflammatory response with increased IL-1β, TNF-α, IL-6, G-CSF and GM-CSF secretion SE-monocytes were relatively refractory to LPS stimulation and failed to produce IL-1β, IL-10, IL-13 or TNF-α (**Figure 7A-C**). In contrast RT-monocytes responded to LPS with increased secretion of CCL3, CCL4, CCL2 and CCL5 as well as a marked increase in IL-1β and TNF-α secretion. Thus, SE-monocytes display phagocytosis, poor T cell stimulation and resistance to LPS whereas RT-monocytes are proinflammatory and able to activate T cells (**Figure 7A-C**).

Functional disparities between RT and SE-monocytes are reflected by extensive transcriptional differences.

To get a more profound insight into the effects of TEM on monocytes we analyzed transcriptional differences between RT and SE-monocytes belonging to the different subsets. Intermediate $CD14^{++}CD16^{+}$ contained the most distinct gene signature with 432 genes more than 10-fold upregulated and 1179 genes more than 10-fold downregulated when comparing SE and RT-monocytes whereas around 200 genes were differentially expressed (> 10-fold) between SE and RT-monocytes in both $CD14^{++}CD16^{-}$ and $CD14^{+}CD16^{++}$ monocytes. RT-monocytes originating from all subsets displayed increased CCL3, CCL4, CXCL1, CXCL2 and IL-8, and proinflammatory genes including TNF family members and IL-1 compared with SE-monocytes. CD14, which is typically maintained in macrophages that do not follow the DC-pathway, was consistently upregulated on SE-monocytes of all subsets. In line with the immunosuppressive phenotype of SE-monocytes they expressed 15-fold higher levels of SIGLEC-7, a marker of anti-inflammatory macrophages (**supp. Table 1-3**).

Discussion

Liver macrophages are a heterogeneous population derived from monocytes recruited via the blood and a sessile population of resident Kupffer cells, that arise from local precursors.(24) In inflammatory liver disease SE-monocytes are recruited in increased numbers from the blood and differentiate into distinct functional subsets of DCs that activate adaptive responses and macrophages that regulate inflammation, fibrogenesis and resolution.(25) In order to be recruited from blood monocytes must undergo TEM across hepatic endothelium before entering tissue and because sinusoidal endothelium can modulate T cell activation we proposed that TEM might affect the subsequent differentiation and function of monocytes. Recent evidence shows that monocytes can exit inflamed tissues

into blood by reverse transmigration from the abluminal to luminal side of the endothelium, a process that may also have a major effect on differentiation and function and which has been proposed as a route for DC emigration from the liver into lymph nodes.(26)

We used a model system incorporating human HSEC to show for the first time that monocytes are able to undergo bidirectional migration through hepatic endothelium with a significant number of transmigrated monocytes migrating back in the abluminal to luminal direction. Migratory stimuli from activated liver stromal cells presumably augment monocyte recruitment. Migration in both directions was partly dependent on JAK-STAT signaling confirming that it is an active process. We suggest that these processes are likely to be highly relevant to immune surveillance and inflammatory responses because they determine the function of the cells and give rise to important differences between tissue monocytes and those that exit the liver through reverse transmigration and may then enter draining lymph nodes.

The phenotype of SE-monocytes ($CD163^{lo}$, $HLA\text{-}DR^{hi}$, $CD86^{med}$ and $CD83^{neg}$) was reminiscent of subsets of hepatic monocyte-derived macrophages described earlier.(10) Furthermore, monocytes that remained in the subendothelial compartment demonstrated high phagocytic activity, were largely refractory to LPS treatment and failed to stimulate T-cell activation whereas RT-monocytes were proinflammatory and induced robust $CD4^+$ T-cell activation and proliferation. This is consistent with previous experiments using umbilical vein endothelial cells in which $CD16^+$ migratory pre-DCs undergo reverse transmigration and in which postmigratory monocytes exhibit features of foam cell macrophages.(17, 27) In our study the RT-monocytes were $CD16^+$ and experiments in which the starting population consisted of highly pure subsets confirmed that some $CD16^-$ cells can became $CD16^+$ during the process of RT. This suggests that CD16 expression is associated with a migratory phenotype and transcriptome analysis of these cells showed that they secrete a range of chemokines which could be involved in autocrine or paracrine migratory responses. The $CD14^{++}CD16^-$ monocytes that failed to undergo reverse TEM expressed higher levels of

STAT2, which is known to counteract differentiation of monocytes to DCs and these cells engulfed more zymosan particles than the $CD16^+$ cells that underwent RT consistent with a macrophage phagocytic function. (18)

We found that TEM across HSEC modulates cellular function and phenotype rather than simply selecting pre-existing subsets. $CD14^{++}CD16^-$ monocytes gained CD16 expression during reverse transmigration from the basal to apical side of the endothelium and showed reduced inflammatory cytokine secretion when residing in the subendothelial matrix. 'Non-classical' $CD16^{hi}$ monocytes have been reported to be highly motile, crawling along blood vessels, and have the highest capacity to elicit T-cell proliferation.(28) We found that a considerable proportion of this subset undergoes reverse transmigration and gains the ability to activate T cells indicating DC functions. This suggests that after capturing tissue antigens they undergo reverse TEM and migrate to draining lymph nodes either via the parasinusoidal route described by Matsuno or via blood and high endothelial venules where they activate T cell responses.(26)

Many non-parenchymal hepatic cells including DCs, HSEC and Kupffer cells display immunosuppressive properties.(31, 32) Our data suggest that monocytes that cross sinusoidal endothelium and are then retained in the subendothelial space contribute to the tolerogenic liver environment because they were unable to efficiently activate T cells in response to viral or alloantigens. In fact, they suppressed $CD4^+$ T-cell proliferation and were refractory to activation via TLR4 similar to entotoxin-tolerant liver myeloid DCs.(29) In terms of their poor ability to activate T-cells SE-monocytes in our model share some properties with human liver $CD11c^+CD11b^+BDCA1^+$ myeloid DCs.(30) Nevertheless, we did not observe induction of IL-10 producing regulatory T-cells nor Th2 skewed immune response as has been described for liver DCs but rather suppression of activation and proliferation associated with increased expression of *NFATC2*.(30-32) These results provide more evidence to support the hypothesis that efficient T cell activation in the liver occurs in draining lymph nodes whereas activation in the liver itself leads to tolerance.(33) Such a mechanism could

contribute to the exhaustion and disappearance of $CD4^+$ T-cell responses seen in viral hepatitis.(34) $CD14^{++}CD16^-$ SE-monocytes showed a 70-fold upregulation of *HLA-E* mRNA transcription compared to RT-monocytes. HLA-E is a ligand for the inhibitory NK-cell ligand CD94/NKG2A suggesting another potential anti-inflammatory mechanism employed by SE-monocytes.(35)

Unlike myeloid-derived suppressor cells, SE-monocytes were MHC-II^{hi} and expressed high cell surface levels of the co-stimulatory molecule CD86 and low levels of PDL-1, which can induce T-cell-apoptosis. Consistent with this PD-1 and CTLA-4 were not up-regulated in $CD4^+$ T-cells stimulated with SE-monocytes and the T cells did not show evidence of apoptosis. The molecular mechanisms through which SE-monocytes suppress $CD4^+$ T-cell activation warrant further investigation.

In contrast to their subendothelial counterparts RT-monocytes induced a robust autologous and allogeneic $CD4^+$ T-cell response characterized by IFN-γ secretion, T-cell activation and proliferation. Our model recapitulates the translocation of migratory hepatic DC to the draining afferent secondary tissue that has been described in rats.(26) That HSEC can induce such functionally different responses suggests that monocyte/HSEC interactions contribute to the balance between systemic immune activation and local suppression of inflammatory processes within the liver. In some respects RT-monocytes from our experiments resemble monocyte-derived TNF-α/iNOS-producing inflammatory DCs that take up antigens in peripheral tissue before migrating to the lymph node and releasing inflammatory cytokines.(36, 37) RT-monocytes secreted proinflammatory mediators after LPS stimulation consistent with a proinflammatory phenotype and expressed high levels of *MYD88*, which links TLR-mediated signals to NFκB activation. Of note, some genes were expressed by all RT-monocytes regardless of their CD14/CD16 status. These included *CCL3*, *CCL4* and *IL1B*, suggesting that reverse transmigration itself activates a specific pattern of genes in originally distinct subpopulations.

Functionally RT and SE-monocytes resembled $CD16^-$ and $CD16^+$ subsets respectively, due to overlapping patterns of cytokine response upon LPS challenge for example.(38,39) However, meticulous transcriptome analysis of highly pure sorted subsets indicated that the monocyte phenotypes described here are not a consequence of selection of pre-existing subsets by HSEC but driven by the transmigration process itself, given the vast differences between RT and SE-monocytes derived from the same subset.

In summary, the outcome of monocyte/HSEC interactions is dichotomous and yields immunogenic DC-like cells that potentially drive systemic immune response but also cells that resemble regulatory macrophages that dampen local inflammation. We provide evidence that the retention of immunosuppressive macrophages might be a unique feature of the hepatic endothelium. Thereby, we provide a novel mechanism through which sinusoidal endothelial cells can regulate the balance between immunity and tolerance.

Acknowledgements:

We thank the staff at the Liver Transplant Unit, Queen Elizabeth Hospital Birmingham, UK for their help with sample collection and the patients for donating blood and tissue. We also thank Gill Muirhead and Janine Youster for their help with HSEC isolation and culture, Miroslava Blahova for the excellent general technical support and Stephen Kissane for performing SAGE analysis.

References:

1. Auffray C, Fogg D, Garfa M, Elain G, Join-Lambert O, Kayal S, Sarnacki S, et al. Monitoring of blood vessels and tissues by a population of monocytes with patrolling behavior. Science 2007;317:666-670.
2. Randolph GJ, Inaba K, Robbiani DF, Steinman RM, Muller WA. Differentiation of phagocytic monocytes into lymph node dendritic cells in vivo. Immunity 1999;11:753-761.
3. Randolph GJ, Beaulieu S, Lebecque S, Steinman RM, Muller WA. Differentiation of monocytes into dendritic cells in a model of transendothelial trafficking. Science 1998;282:480-483.
4. Varol C, Landsman L, Fogg DK, Greenshtein L, Gildor B, Margalit R, Kalchenko V, et al. Monocytes give rise to mucosal, but not splenic, conventional dendritic cells. J Exp Med 2007;204:171-180.
5. Varol C, Yona S, Jung S. Origins and tissue-context-dependent fates of blood monocytes. Immunol Cell Biol 2009;87:30-38.
6. Ziegler-Heitbrock L, Ancuta P, Crowe S, Dalod M, Grau V, Hart DN, Leenen PJ, et al. Nomenclature of monocytes and dendritic cells in blood. Blood 2010;116:e74-80.
7. Grage-Griebenow E, Flad HD, Ernst M. Heterogeneity of human peripheral blood monocyte subsets. J Leukoc Biol 2001;69:11-20.
8. Karlmark KR, Weiskirchen R, Zimmermann HW, Gassler N, Ginhoux F, Weber C, Merad M, et al. Hepatic recruitment of the inflammatory Gr1+ monocyte subset upon liver injury promotes hepatic fibrosis. Hepatology 2009;50:261-274.
9. Klein I, Cornejo JC, Polakos NK, John B, Wuensch SA, Topham DJ, Pierce RH, et al. Kupffer cell heterogeneity: functional properties of bone marrow derived and sessile hepatic macrophages. Blood 2007;110:4077-4085.
10. Liaskou E, Zimmermann HW, Li KK, Oo YH, Suresh S, Stamataki Z, Qureshi O, et al. Monocyte subsets in human liver disease show distinct phenotypic and functional characteristics. Hepatology 2013;57:385-398.
11. Shetty S, Lalor PF, Adams DH. Lymphocyte recruitment to the liver: molecular insights into the pathogenesis of liver injury and hepatitis. Toxicology 2008;254:136-146.
12. Lalor PF, Lai WK, Curbishley SM, Shetty S, Adams DH. Human hepatic sinusoidal endothelial cells can be distinguished by expression of phenotypic markers related to their specialised functions in vivo. World J Gastroenterol 2006;12:5429-5439.
13. Carambia A, Frenzel C, Bruns OT, Schwinge D, Reimer R, Hohenberg H, Huber S, et al. Inhibition of inflammatory CD4 T cell activity by murine liver sinusoidal endothelial cells. J Hepatol 2013;58:112-118.
14. Carambia A, Freund B, Schwinge D, Heine M, Laschtowitz A, Huber S, Wraith DC, et al. TGF-beta-dependent induction of CD4(+)CD25(+)Foxp3(+) Tregs by liver sinusoidal endothelial cells. J Hepatol 2014;61:594-599.
15. Liaskou E, Karikoski M, Reynolds GM, Lalor PF, Weston CJ, Pullen N, Salmi M, et al. Regulation of mucosal addressin cell adhesion molecule 1 expression in human and mice by vascular adhesion protein 1 amine oxidase activity. Hepatology 2011;53:661-672.
16. Aspinall AI, Curbishley SM, Lalor PF, Weston CJ, Miroslava B, Liaskou E, Adams RM, et al. CX(3)CR1 and vascular adhesion protein-1-dependent recruitment of CD16(+) monocytes across human liver sinusoidal endothelium. Hepatology 2010;51:2030-2039.
17. Randolph GJ, Sanchez-Schmitz G, Liebman RM, Schakel K. The CD16(+) (FcgammaRIII(+)) subset of human monocytes preferentially becomes migratory dendritic cells in a model tissue setting. J Exp Med 2002;196:517-527.
18. Lee D, Lee HS, Yang SJ, Jeong H, Kim DY, Lee SD, Oh JW, et al. PRSS14/Epithin is induced in macrophages by the IFN-gamma/JAK/STAT pathway and mediates transendothelial migration. Biochem Biophys Res Commun 2011;405:644-650.
19. Platt AM, Randolph GJ. Dendritic cell migration through the lymphatic vasculature to lymph nodes. Adv Immunol 2013;120:51-68.

20. Hume DA, MacDonald KP. Therapeutic applications of macrophage colony-stimulating factor-1 (CSF-1) and antagonists of CSF-1 receptor (CSF-1R) signaling. Blood 2012;119:1810-1820.
21. Abe BT, Shin DS, Mocholi E, Macian F. NFAT1 supports tumor-induced anergy of CD4(+) T cells. Cancer Res 2012;72:4642-4651.
22. Shin DS, Jordan A, Basu S, Thomas RM, Bandyopadhyay S, de Zoeten EF, Wells AD, et al. Regulatory T cells suppress CD4+ T cells through NFAT-dependent transcriptional mechanisms. EMBO Rep 2014.
23. Green DR, Droin N, Pinkoski M. Activation-induced cell death in T cells. Immunol Rev 2003;193:70-81.
24. Tacke F, Zimmermann HW. Macrophage heterogeneity in liver injury and fibrosis. J Hepatol 2014;60:1090-1096.
25. Iredale JP. Models of liver fibrosis: exploring the dynamic nature of inflammation and repair in a solid organ. J Clin Invest 2007;117:539-548.
26. Matsuno K, Ezaki T, Kudo S, Uehara Y. A life stage of particle-laden rat dendritic cells in vivo: their terminal division, active phagocytosis, and translocation from the liver to the draining lymph. J Exp Med 1996;183:1865-1878.
27. Westhorpe CL, Dufour EM, Maisa A, Jaworowski A, Crowe SM, Muller WA. Endothelial cell activation promotes foam cell formation by monocytes following transendothelial migration in an in vitro model. Exp Mol Pathol 2012;93:220-226.
28. Cros J, Cagnard N, Woollard K, Patey N, Zhang SY, Senechal B, Puel A, et al. Human CD14dim monocytes patrol and sense nucleic acids and viruses via TLR7 and TLR8 receptors. Immunity 2010;33:375-386.
29. Thomson AW, Knolle PA. Antigen-presenting cell function in the tolerogenic liver environment. Nat Rev Immunol 2010;10:753-766.
30. Bamboat ZM, Stableford JA, Plitas G, Burt BM, Nguyen HM, Welles AP, Gonen M, et al. Human liver dendritic cells promote T cell hyporesponsiveness. J Immunol 2009;182:1901-1911.
31. Khanna A, Morelli AE, Zhong C, Takayama T, Lu L, Thomson AW. Effects of liver-derived dendritic cell progenitors on Th1- and Th2-like cytokine responses in vitro and in vivo. J Immunol 2000;164:1346-1354.
32. Jinushi M, Takehara T, Tatsumi T, Yamaguchi S, Sakamori R, Hiramatsu N, Kanto T, et al. Natural killer cell and hepatic cell interaction via NKG2A leads to dendritic cell-mediated induction of CD4 CD25 T cells with PD-1-dependent regulatory activities. Immunology 2007;120:73-82.
33. Barbier L, Tay SS, McGuffog C, Triccas JA, McCaughan GW, Bowen DG, Bertolino P. Two lymph nodes draining the mouse liver are the preferential site of DC migration and T cell activation. J Hepatol 2012;57:352-358.
34. Schulze Zur Wiesch J, Ciuffreda D, Lewis-Ximenez L, Kasprowicz V, Nolan BE, Streeck H, Aneja J, et al. Broadly directed virus-specific CD4+ T cell responses are primed during acute hepatitis C infection, but rapidly disappear from human blood with viral persistence. J Exp Med 2012;209:61-75.
35. Nattermann J, Nischalke HD, Hofmeister V, Ahlenstiel G, Zimmermann H, Leifeld L, Weiss EH, et al. The HLA-A2 restricted T cell epitope HCV core 35-44 stabilizes HLA-E expression and inhibits cytolysis mediated by natural killer cells. Am J Pathol 2005;166:443-453.
36. Serbina NV, Salazar-Mather TP, Biron CA, Kuziel WA, Pamer EG. TNF/iNOS-producing dendritic cells mediate innate immune defense against bacterial infection. Immunity 2003;19:59-70.
37. Sunderkotter C, Nikolic T, Dillon MJ, Van Rooijen N, Stehling M, Drevets DA, Leenen PJ. Subpopulations of mouse blood monocytes differ in maturation stage and inflammatory response. J Immunol 2004;172:4410-4417.
38. Belge KU, Dayyani F, Horelt A, Siedlar M, Frankenberger M, Frankenberger B, Espevik T, et al. The proinflammatory CD14+CD16+DR++ monocytes are a major source of TNF. J Immunol 2002;168:3536-3542.

39. Ziegler-Heitbrock HW, Strobel M, Kieper D, Fingerle G, Schlunck T, Petersmann I, Ellwart J, et al. Differential expression of cytokines in human blood monocyte subpopulations. Blood 1992;79:503-511.

Figure legends

Figure 1. Hepatic sinusoidal endothelial cells favour recruitment and subendothelial accumulation of $CD14^+$ monocytes. (A) Schematic illustration of a tissue model to study TEM of monocytes. Primary HSEC isolated from explanted livers were seeded onto a collagen 3D matrix with an interposed fibronectin thin layer and grown to confluence. The HSEC monolayer was stimulated with 10 ng/mL of TNF-α /IFN-γ for 24h to enhance immune cell recruitment, followed by the addition of freshly purified $CD14^+$ monocytes. Non-migrating cells were discarded and the co-culture was continued for a total of 48h. During this period spontaneous reverse transmigration across HSEC of a minor fraction of monocytes occurred with the majority arising from resident subendothelial monocytes. (B) Collagen matrix was supplemented with FITC-labelled zymosan particles. Representative contour plots indicate the differential phagocytic capacity RT and SE-monocytes after 48h of cultivation and the impact on CD16 expression. (C) Comparison of quantitative RT/SE monocyte distribution after bidirectional TEM across either HSEC or HUVEC. Mean and SEM from 3 independent experiments; *P* values from unpaired t-test.

Figure 2. Reverse transmigrating monocytes are mainly composed of $CD14^{++}CD16^+$ monocytes and originate from $CD16^+$ and $CD16^-$ precursor cells (A). Composition of RT and SE-monocytes according to differential CD14 and CD16 expression. The percentage of 'classical' $CD14^{++}CD16^-$, 'intermediate' $CD14^{++}CD16^+$ and 'non-classical' $CD14^+CD16^{++}$ monocyte among RT and SE-monocytes is shown for each experiment (n=7 independent experiments with HSEC and monocytes from different donors; P values from paired-test). (B) Representative zebra plots of peripheral monocyte subset distribution prior to FACS sorting (left figure) and CD14/CD16 expression of sorted monocyte subsets after 48h of bidirectional TEM across HSEC (right figures). (C) Stacked columns depicting percentages of SE and RT

fractions for each monocyte subset (mean and SEM from N=3 independent experiments) (bottom left figure).

Figure 3. Reverse transmigrating cells exhibit a phenotype reminiscent of immature dendritic cells. Depiction of representative histograms / density plots from flow cytometry of various surface markers implicated in macrophage / DC phenotype on RT (black line) and SE-monocytes (light grey). Isotype-matched controls highlighted in dark grey. Bar graphs represent mean fluorescence intensity (MFI) (mean, SEM, p-value of paired t-test).

Figure 4. RT-monocytes mount efficient $CD4^+$ T-cell proliferative responses whereas SE monocyte elicit T-cell suppression. (A) Representative CFSE plots of proliferating autologous CD4+ T-cells after antigen-specific stimulation with RT vs. SE-monocytes at monocyte / T-cell ratios of 1:50 to 1:5 (left panel). Quantification of proliferating autologous $CD4^+$ T-cells after Ag-specific stimulation with RT-monocytes (red) and SE-monocytes (blue) given as percentage of total cells (mean, SEM from n=3 independent experiments) (right figure). (B) Quantification of proliferating allogeneic $CD4^+$ T-cells after stimulation with RT-monocytes (red) vs. SE-monocytes (blue) in a T cell suppression assay given as percentage of total cells (mean, SEM from n=5 independent experiments). (C) Representative CFSE plots of proliferating $CD4^+$ T-cells after stimulation with immobilized α-CD3 Ab (OKT3) in the presence of RT vs. SE-monocytes at T-cell / monocyte ratios of 4:1 to 1:4 (left panel). Quantification of n=3 independent experiments (mean, SEM) comparing proliferation capacity of OKT3-stimulated CD4+ T-cells in the presence of RT (red) vs. SE-monocytes (green). CD3/CD28 bead stimulated $CD4^+$ T-cells co-cultured with SE-monocytes are highlighted in blue. Dotted line represents baseline $CD4^+$ T-cell proliferation without OKT3 in the absence of monocytes. Dashed line indicates OKT3-stimulated CD4+ T-cell proliferation without monocytes (right figure). (D) Representative FACS plot of Annexin V assay after 5d of Ag-specific autologous $CD4^+$ T-cell stimulation with RT vs. SE-monocytes, gated on $CD4^+$

T-cells. Lower right quadrant represents early apoptotic cells, cells in top right quadrant are late apoptotic / necrotic.

Figure 5. RT-monocytes are capable of inducing $CD4^+$ T-cell activation whereas SE counterparts promote anergy in autologous T-cells. (A) Schematic illustration of experiments assessing autologous $CD4^+$ T-cell activation by RT and SE-monocytes. After retrieval of SE and RT-monocytes of CMV seropositive donors, cells were cultivated with pp65 CMV Ag for 24h, autologous $CD4^+$ T-cell were added and co-cultured for 5d at monocyte / T-cell ratios of 1:5 and 1:10 in the presence of recombinant IL-2 (50 IU/mL). (B) Representative FACS dot plots of CD25, CD26, CD69, CD71 and HLA-DR expression on $CD4^+$ T-cells after 60h of co-culture with RT and SE-monocytes or without monocytes. (C) Quantification of T-cell activation marker expression. Bar graphs represent percentage of positive cells (mean and SEM of 3 to 4 independent experiments, p values from Bonferroni's post hoc test). (D) Transcriptional regulation of genes involved in T helper cell polarization in $CD4^+$ T-cells from a CMV seropositve donor stimulated with autologous CMV pp65 bearing SE vs. RT-monocytes. Genes with at least two-fold regulation are indicated.

Figure 6. RT-monocytes induce multifaceted T-cell response patterns whereas SE-monocytes promote $CD4^+$ T-cell anergy. (A) Representative FACS plot of intracellular IFN-γ expression after Ag-specific stimulation of autologous $CD4^+$ T-cells with RT vs. SE-monocytes (left panel). Bar graphs depicting quantification of n=9 experiments (mean, SEM, p value from paired t-test) (right figure). (B) Exemplary FACS plots of intracellular CTLA-4 (y-axis) and FOXP3 (x-axis) in $CD4^+$ T-cells co-incubated with either RT or SE-monocytes (left panel) Representative histogram of intracellular CTLA-4 expression (grey line denoting isotype control, dark line denoting $CD4^+$ T-cells stimulated by SE-monocytes, grey fill denoting $CD4^+$ T-cells stimulated by RT-monocytes) and respective statistical analysis. (mean of MFI, SEM, n=4 experiments) (right panel). (C) Representative FACS plots of

intracellular IL-4 (y-axis) and IL-10 expression (x-axis) after Ag-specific stimulation of autologous CD4+ T-cells with RT vs. SE-monocytes (left panel). Bar graphs illustrating percentage of IL-10 positive $CD4^+$ T-cells (mean, SEM, n=5 experiments). (D) Representative histogram of PD-L1 surface expression on RT vs. SE-monocytes (left figure) and respective statistical analysis (mean of MFI, SEM, n=5, p value from paired t-test) (right figure). (E) Statistical analysis of PD-1 expression on CD4+ T-cells stimulated with RT vs. SE-monocytes (mean, SEM, n=6 experiments, p value from paired t-test). (F) Representative contour plot of intracellular CTLA-4 (y-axis) and IFN-γ (x-axis) expression in $CD4^+$ T-cells that were stimulated with SE monocytes after TEM across HSEC vs. HUVEC.

Figure 7: Differential release of cytokines / chemokines upon LPS stimulation highlights endotoxin resistance of SE-monocytes. 1.2 x 10^5 SE or RT-monocytes were stimulated with either 10 ng/mL of LPS or left unstimulated for 24h in serum-free medium. Conditioned media was analyzed for the secretion of chemokines and cytokines. (A) Representative images of nitrocellulose membranes with spotted antibodies against several cytokines and densitometric quantification (normalized mean pixel density of chemiluminescence) of those (B) cytokines and (C) chemokines in supernatants from unstimulated RT (white) / SE (dark grey) and stimulated RT (light grey) and SE-monocytes (black). In (A) reference spots for normalization are highlighted by white boxes.

Figure 8: Diagram of the proposed mechanism. Diapedesis across hepatic sinusoidal endothelial cells shapes functional outcome of monocytes that enter the liver via blood stream. All three monocyte subsets can transmigrate with the $CD14^+CD16^-$ subset being mostly confined to reside in the subendothelial layer (space of Dissé) whilst $CD16^+$ monocytes can undergo reverse transmigration. Activated liver myofibroblasts (aLMF) support both recruitment of monocytes as well as as intrahepatic retention of monocytes

through soluble factors. Subendolthelial (SE) monocytes are highly phagocytic and display a macrophage-like phenotype. Upon LPS stimulation SE monocytes fail to mount a relevant proinflammatory response (LPS tolerance) and promote $CD4^+$ T-cell anergy by restraining cell activation and proliferation thereby dampening local immune reactions. In turn, reverse transmigrating (RT) monocytes exhibit features of immature dendritic cells and probably employ CCR8 to exit the liver. RT monocytes are potent antigen-presenting cells and release a broad spectrum of proinflammatory cytokines and chemokines upon LPS exposure, which enables a robust induction of $CD4^+$ T-cell proliferation/activation governing a Th1-prone immune response and microenvironment.

Figure 1

Manuscript Number: HEP-15-1041

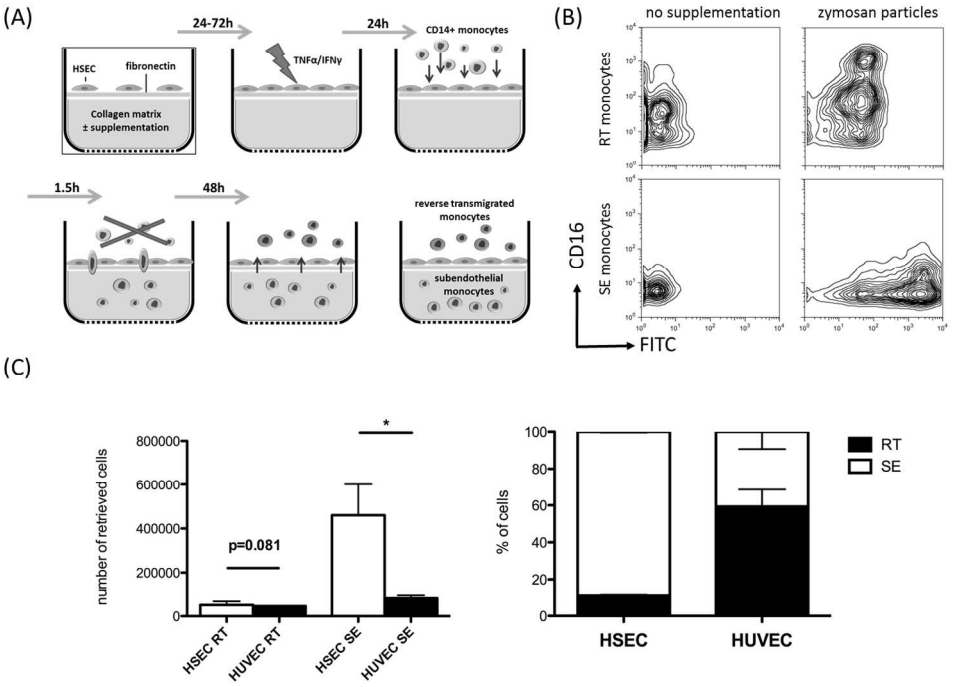

256x191mm (300 x 300 DPI)

Figure 2

Manuscript Number: HEP-15-1041

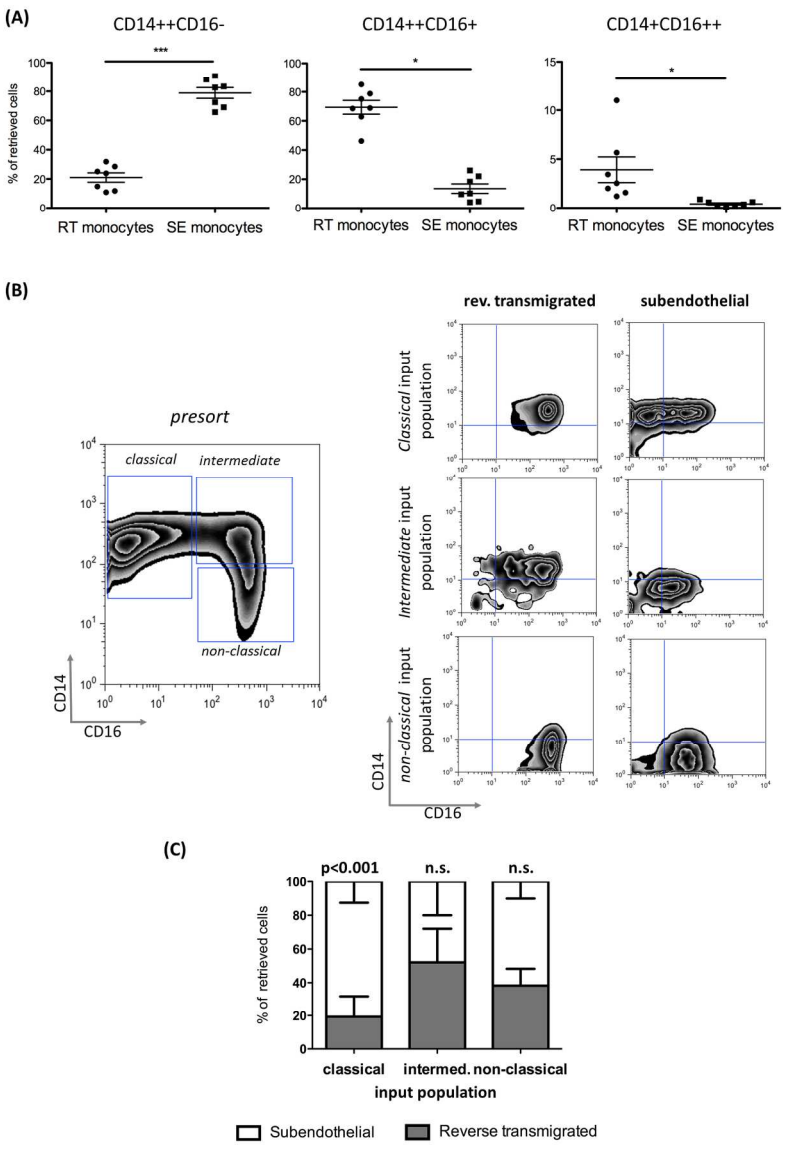

256x385mm (300 x 300 DPI)

Figure 3

Manuscript Number: HEP-15-1041

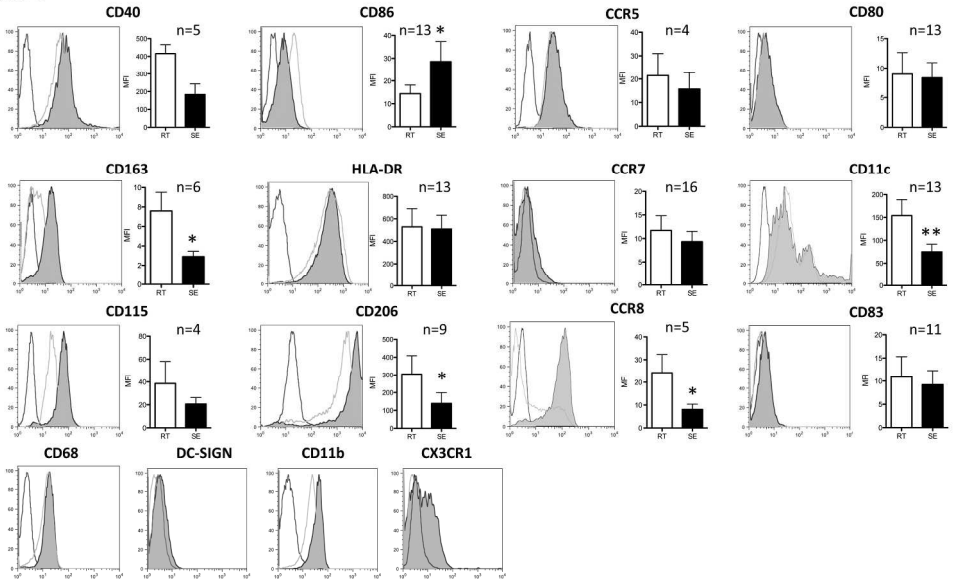

441x267mm (300 x 300 DPI)

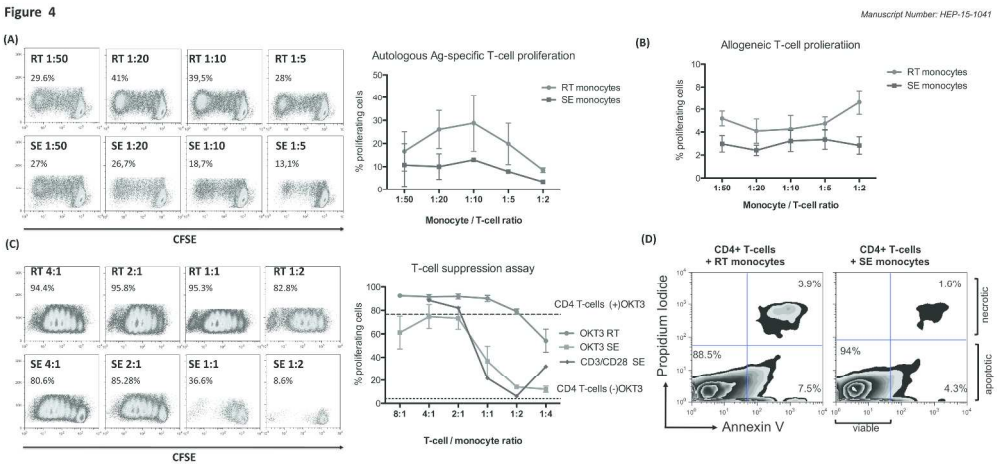

579x270mm (300 x 300 DPI)

Manuscript Number: HEP-15-1041

Figure 5

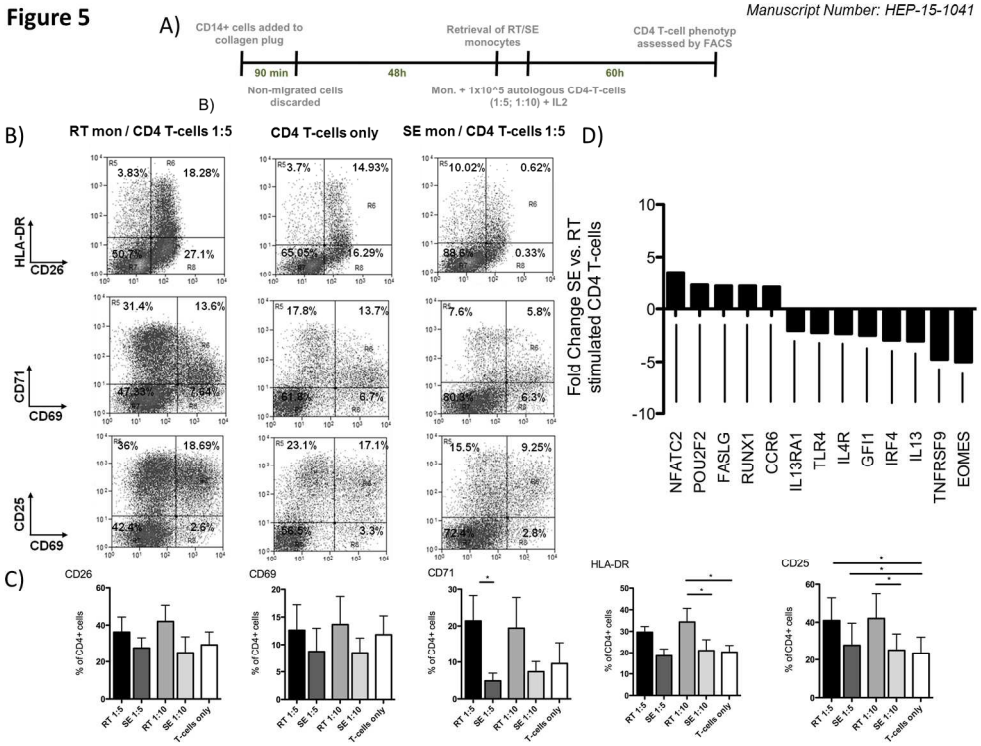

330x249mm (300 x 300 DPI)

Manuscript Number: HEP-15-1041

Figure 6

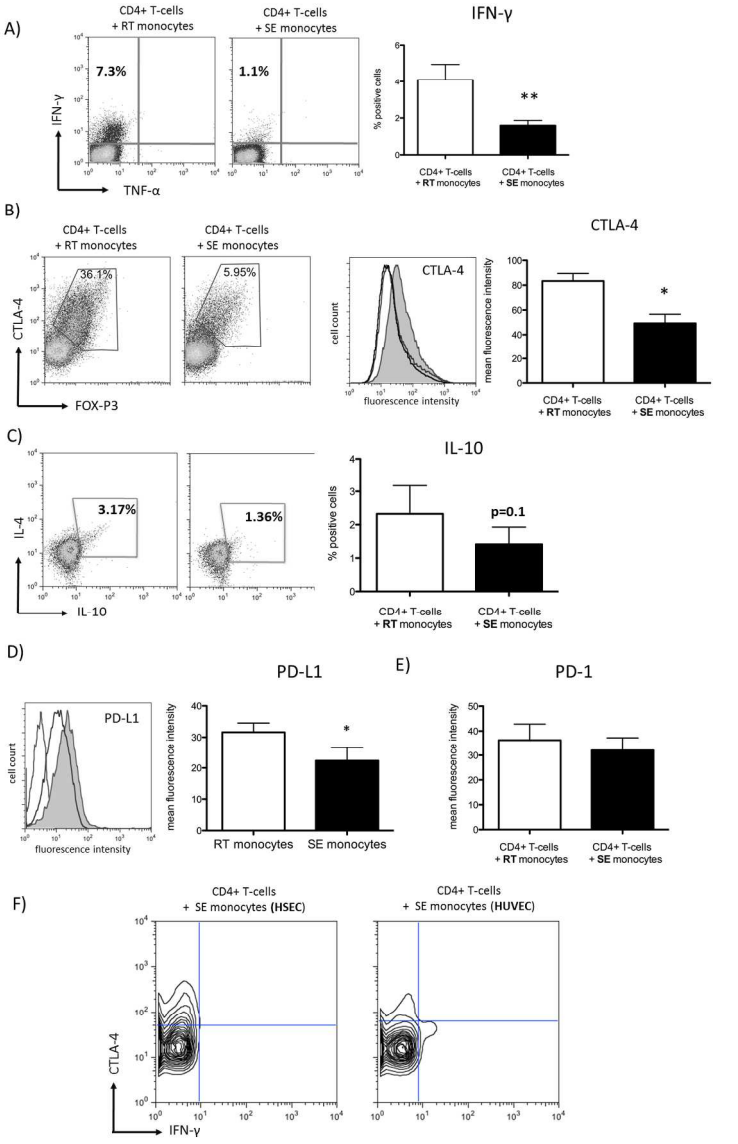

256x398mm (300 x 300 DPI)

Figure 7

Manuscript Number: HEP-15-1041

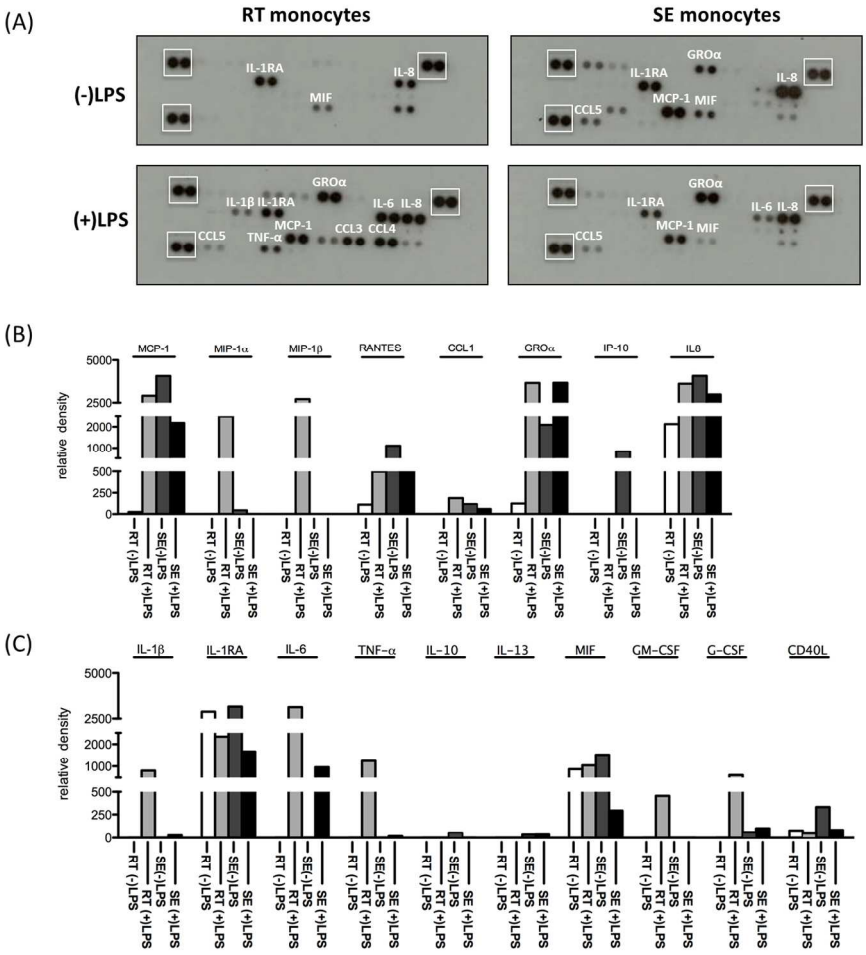

255x261mm (300 x 300 DPI)

Figure 8

Manuscript Number: HEP-15-1041

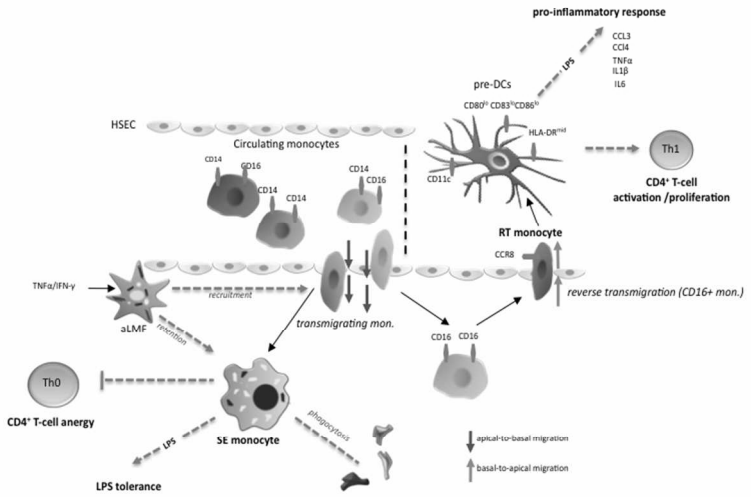

352x264mm (72 x 72 DPI)

Manuscript Number: HEP-15-1041

Supporting Data:

Supplemtentary Materials and Methods:

Isolation and culture of human umbilical vein endothelial cells (HUVEC)

Tissue was collected at the Birmingham Women's Hospital after informed consent and approval by the local research ethics committee. HUVEC were isolated via collagenase digestion and umbilical cords according to standard procedures and cultured to confluence in Human umbilical vein cells were cultured in complete endothelial media containing 10% human AB serum (HD supplies, UK), 10 ng/ml epidermal growth factor (Peprotec, UK) and 10 mg/ml hydrocortisone (Sigma, UK).

Immune Cell Isolation:

Blood was obtained from healthy volunteers and CMV seropositive donors. Mononuclear cells were isolated using established methods.(16) and monocytes purified using MACS isolation and CD14 microbeads and $CD4^+$ T-cells using CD4 microbeads (Miltenyi Biotec, Bergisch-Gladbach, Germany) . Cells were >95% pure by flow cytometry. For proliferation/suppression assays $CD4^+$ T-cells were labeled with CellTrace CFSE Cell Proliferation (Life Technologies) for 10 min with two subsequent quenching steps. To purify monocyte subsets monocytes were enriched using OptiPrep density gradient centrifugation and $CD14^{++}CD16^-$, $CD14^{++}CD16^+$ and $CD14^+CD16^{++}$ monocytes isolated by high-speed flow cytometric sorting after blocking Fc receptors with normal mouse Ig using conjugated mAb against CD14, CD16, and CD15/CD56 (BioLegend) (to exclude contaminating neutrophils and NK-cells) followed by sorting using a MoFlo cell sorter (Beckman-Coulter).

Isolation of aLMF and generation of conditioned medium

Fifty grams of liver was diced and digested using type-1A collagenase (0.4 _g/mL; Sigma Aldrich Ltd, Dorset, UK) followed by mechanical homogenization in a Stomacher 400 Circulator (Seward, NY). The cell suspension was layered over 33/77 (wt/vol) Percoll (Amersham Biosciences, Bucks, UK) gradient and centrifuged for 20 minutes at 2300 rpm. Nonparenchymal cells at the interface were retrieved and fibroblasts were purified by negative immunomagnetic selection. Cholangiocytes and endothelium were removed by immunomagnetic selection with antibodies against HEA-125 (10 _g/mL; Progen Biotechnik, Germany), CD31 (10 _g/mL clone JC-07; DAKO, Dorset, UK), and sheep anti-mouse Dynabeads (Dynal A.S., Norway). aLMF were plated in gelatin-coated flasks in Dulbecco's modified Eagle medium/10% fetal calf serum and viability was confirmed by trypan blue exclusion. Supernatants were generated by seeding 5×10^4 cells per well onto 24-well plates (Co-Star; Corning, NY) in 500 μL phenol-red–free RPMI-1640/1% BSA containing 2 mmol/L L-glutamine, 60 μg/mL benzylpenicillin, and 100 μg/mL streptomycin (all Sigma, UK). Stimulated supernatants were generated by treating cells for 48 hours with 10 ng/mL tumor necrosis factor α (TNFα), and interferon (IFN)γ (all Pepro-Tech, UK).

Flow cytometry

Cells were washed in FACS buffer, resuspended and labeled with fluorochrome-conjugated Abs at pre-determined dilutions at 4°C in PBS/2% FCS/2 mM EDTA and analyzed on a nine-color Dako Cyan Flow Cytometer using Summit 4.3 software (DakoCytomation, Glostrup, Denmark) and FlowJo 8.7 (TreeStar, Ashland, OR). The following Abs were used for surface staining: CD14, CD16, CD68, CD86, CD80, CD83, CD115, CD163, CD40, CD206, CD209, PD-L1, CD69 (FN50), CD25 (M-A251), CD127 (HIL-7R-M21), CD71 (M-A712), HLA-DR (L243), CD26 (L272), PD-1 (MIH1), αL/CD11a (345913 and HI111), CD11b, CD11c, CCR5 (2D7/CCR5), CCR7 (3D12), CCR8, CX3CR1 (2A9-1), mouse IgG1 (X40 and MOPC-21), mouse IgG2a (G155-178, X39 and MOPC-173), mouse IgG2b (27-35), rat IgG2a (54447),

and rat IgG2b (RTK4530); purchased from BD Pharmingen (Swindon, UK), BioLegend (Cambridge, UK), R&D Systems (Minneapolis, MN), eBioscience (Hatfield, UK), or Dako. Intracellular staining was performed using the Cytofix/Cytoperm Kit (BD Biosciences) with Abs against IFN-γ (B27), IL-4, IL-10 (JES3-19F1) (all BD Pharmingen), CTLA-4 and FoxP3 (236A/E7, eBioscience). Apoptosis and necrosis were detected using Annexin V (FITC) and propidium iodide (BD Pharmingen).

Ag-specific and allogeneic CD4+ T-cell stimulation

For Ag-specific CD4+ T-cell stimulation monocytes from CMV seropositive donors were incubated with CMV pp65 for 24h followed by co-culture with autologous $1x10^5$ CD4+ T-cells in a round-bottomed plate in 1640-RPMI plus 10% FCS, 1% GPS and 50 IU/ml IL-2 at 37 °C, 5% CO_2 for 60h. Different ratios were investigated. Alloreactive T-cell activation was done using allogeneic $CD4^+$ T-cells. Intracellular cytokines in $CD4^+$ T-cells were analysed after 8h Golgi block with Brefeldin. CFSE-labelled CD4+ T-cells were used for proliferation assays.

T-cell suppression assay

CFSE-labelled $1x10^5$ CD4+ T-cells and RT/SE monocytes were co-cultured in 1640 RPMI at different ratios in 96 well round bottom plates in the presence of either CD3/CD28 activating beads (Treg inspector; Miltenyi Biotec) or immobilized CD3 Ab (OKT3) to induce T-cell proliferation at a 1:1 bead to T-cell ratio. Co-culture was maintained at 37°C, 5% CO_2 for 36h and FACS analysis used to quantify $CD4^+$ T-cell proliferation.

RT-PCR

RT^2 Profiler PCR Array Human T Helper Cell Differentiation Kit was used to analyse cDNA synthesized using a RT^2 First Strand Kit from samples isolated by the RNeasy minikit and RT^2 SYBR Green qPCR Mastermix (all Qiagen). Samples were analyzed on a Lightcycler 480 II instrument (Roche, Mannheim, Germany) according to the manufacturer's instruction.

Changes in expression of 84 genes associated with T cell differentiation were determined in CD4 T cells before and after migration using online RT^2 profiler PCR Array Data Analysis version 3.5 with normalization for the housekeeping genes *ACTB*, *B2M*, *GAPDH*, *HPRT1*, and *RPLP0*.

Cytokine Secretion Assay

1.2 x 10^5 Rt or SE monocytes cells were cultured in serum-free RPMI 1640 medium in 24-well plates (Costar) and stimulated with 10 ng/ml LPS (Sigma-Aldrich) or left unstimulated for 24h. Supernatant was harvested and cytokine secretion assessed using a Cytokine Array Kit, Panel A (R&D systems).

Serial analysis of gene expression

Barcoded SAGE sequencing libraries were prepared using a SOLiD SAGE Kit with Barcoding Adaptor Module (Life Technologies) and sequenced using a SOLiD 4 System next generation sequencer (Life Technologies). Sequence reads were mapped to human RefSeq release 59 using the SOLiD SAGE v1.10 mapping tool. Tables of tag counts for each sample were used to determine differentially regulated genes using Empirical analysis of digital gene expression data in R^{16} running in the Bioconductor environment version 2.14. Tags were filtered to select tags in which at least three samples had counts per million greater than three.

Long-term imaging of bidirectional monocytic migration across HSEC

Fibronectin-coated collagen matrix was prepared as described above and added to 24-well plate. 7.5x10^5 primary HSEC were seeded onto polymerized collagen plugs in a 24-well plate and grown confluent and subsequently stimulated with 10 ng/mL TNFα + IFNγ for

24h. Monocytes were purified according to standard procedures. Isolated 2.5x10^5 monocytes were added and co-cultured for >24h. Monocyte migration across HSEC was imaged by a Cell-IQÓ microscope allowing imaging under cell-culture conditions. Pictures were taken every 15 minutes.

Supplemtentary Figure legends:

Supplementary Figure S1: Monocyte TEM across underlies JAK/STAT activation. Freshly purified monocytes were treated with JAK 1 inhibitor or DMSO control at time-point 0 prior to TEM across HSEC. Bar graphs depict results of n=5 independent experiments. (mean, SEM, paired t-test).

Supplementary Figure S2: Activated liver stromal cells augment monocyte recruitment across HSEC and thereby likely expand hepatic macrophage pool during liver disease.
Impact of aLMF conditioned media in the tissue model of bidirectional monocyte TEM. Collagen matrix was supplemented with conditoned media from aLMF ± prior TNF-α/IFN-γ treatment and number of SE and RT monocytes were counted (A) Total number of cells that migrated. TNFa/IFNg supplemented collagen was used to verify that the effects on monocyte transmigration were not mediated by TNFa/IFNg itself. (B) Bar graphs representing the number RT- and SE-monocytes with either non-supplemented or aLMF (± TNF-α/IFN-γ-stimulation) CM supplemented collagen matrixes (C). Stacked bar graphs comparing the relative fraction of RT and SE monocytes. (mean, SEM, n=3 experiments, p value from paired t-test).

Supplementary Table 1: SAGE analysis of transcriptome changes in RT vs SE monocytes from 'classical' CD14++CD16- monocytes. Selection of genes of interest with at least 10-fold regulation between RT and SE monocytes.

Supplementary Table 2: SAGE analysis of transcriptome changes in RT vs SE monocytes from 'intermediate' CD14++CD16+ monocytes. Selection of genes of interest with at least 10-fold regulation between RT and SE monocytes.

Supplementary Table 3: SAGE analysis of transcriptome changes in RT vs SE monocytes from 'non-classical' CD14+CD16++ monocytes. Selection of genes of interest with at least 10-fold regulation between RT and SE monocytes.

Supplementary Figure S1

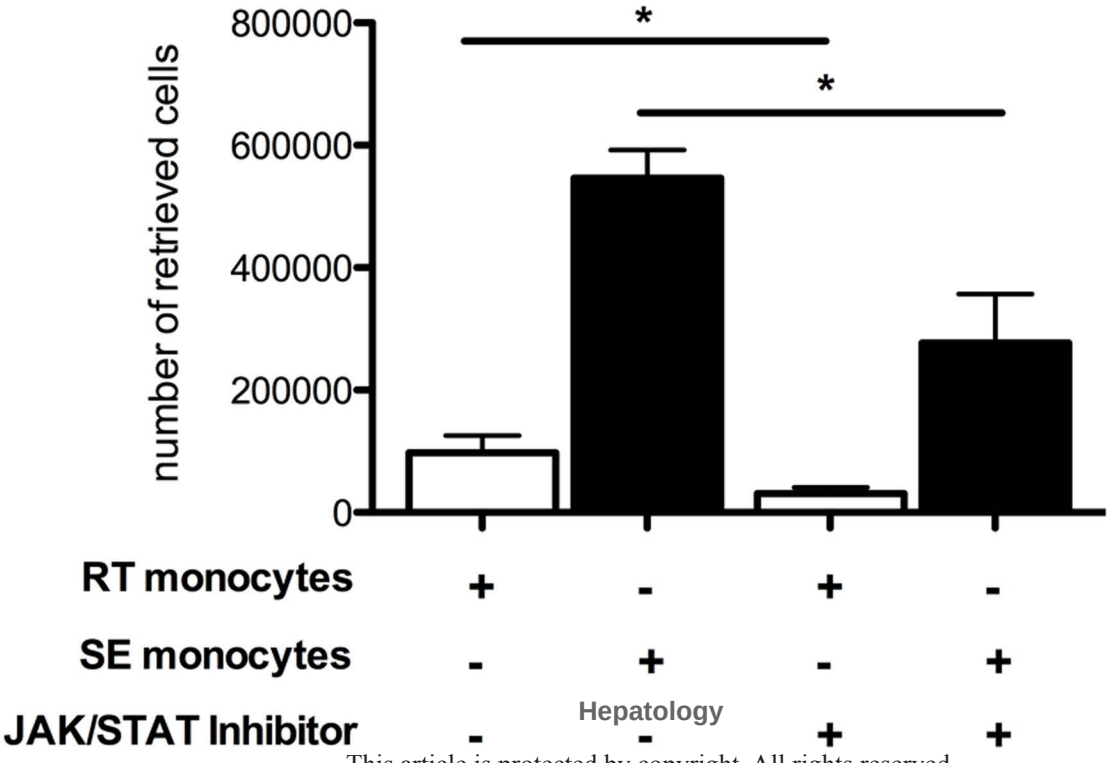

Supplementary Figure S2

Manuscript Number: HEP-15-1041

(A)

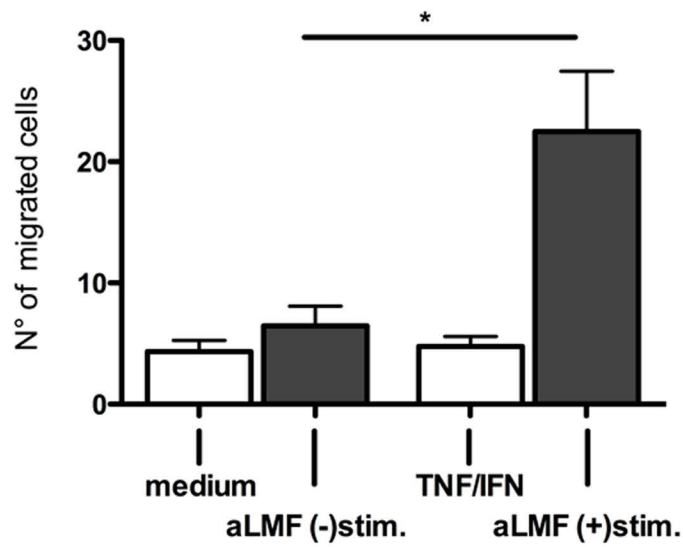

(B)

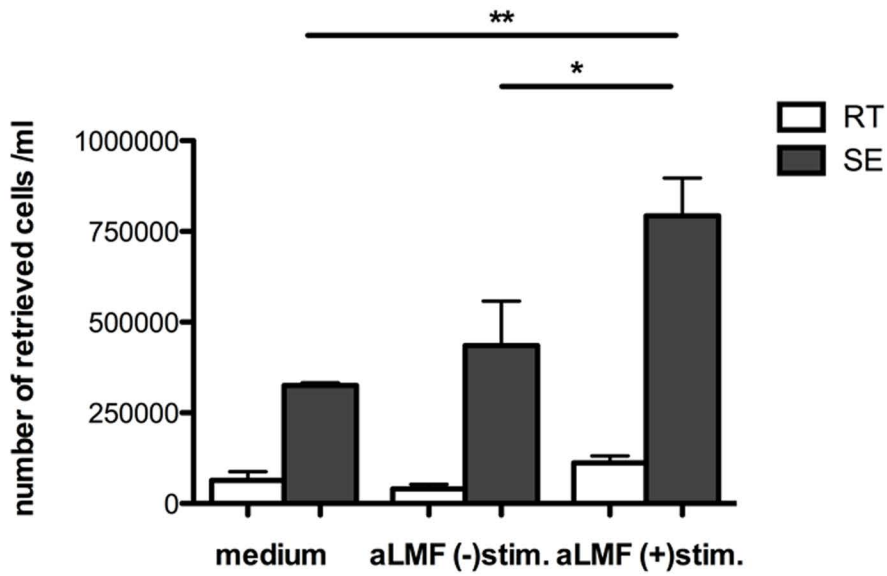

(C)

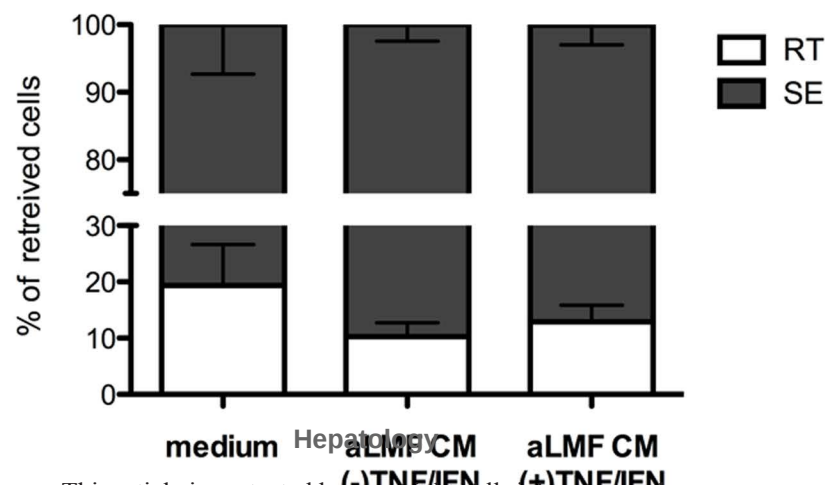

Manuscript Number: HEP-15-1041

Supplementary Table1:

Comparison reverse transmigrating vs. subendothelial CD14++CD16- monocytes	
Higher in SE monocytes	
Fold-change	**Gene**
70.38	Major histocompatibility complex I, E (HLA-E)
21,74	CD14 molecule transcript variant I
19,13	tumor necrosis factor (ligand) superfamily, member 13b (TNFSF13B), transcript variant 1,
18,5216	signal transducer and activator of transcription 2, 113kDa (STAT2), transcript variant 1,
15,7397	sialic acid binding Ig-like lectin 7 (SIGLEC7), transcript variant 3
Higher in RT monocytes	
Fold-change	**Gene**
38,41	tumor necrosis factor (TNF)
29,55	tumor necrosis factor receptor superfamily, member 12A (TNFRSF12A)
28,57	interleukin 8 (IL8)
27,55	chemokine (C-C motif) ligand 3 (CCL3)
24,75	interleukin 1, beta (IL1B)
24,29	chemokine (C-X-C motif) ligand 1 (melanoma growth stimulating activity, alpha) (CXCL1)
22,35	jun proto-oncogene (JUN)
19,48	insulin-like growth factor binding protein 7 (IGFBP7)
18,63	chemokine (C-C motif) ligand 4-like 1 (CCL4L1)
18,36	chemokine (C-C motif) ligand 3-like 3 (CCL3L3)
17,00	CD59 molecule, complement regulatory protein (CD59)
13,64	chemokine (C-X-C motif) ligand 2 (CXCL2)

Manuscript Number: HEP-15-1041

Supplemental Table 2:

Comparison reverse transmigrating vs. subendothelial CD14++CD16+ monocytes	
Higher in SE monocytes	
Fold-change	**Gene**
111,00	S100 calcium binding protein A11 (S100A11)
62,53	CD14 molecule (CD14), transcript variant 1
48,75	major histocompatibility complex, class II, DP beta 1 (HLA-DPB1)
32,54	interferon, gamma-inducible protein 30 (IFI30)
30,85	colony stimulating factor 1 receptor (CSF1R)
29,96	major histocompatibility complex, class II, DQ alpha 1 (HLA-DQA1)
29,65	chemokine (C-X-C motif) ligand 16 (CXCL16), transcript variant 1
29,38	CD63 molecule (CD63), transcript variant 1
28,99	major histocompatibility complex, class II, DR beta 1 (HLA-DRB1)
28,81	suppressor of cytokine signaling 7 (SOCS7)
27,54	interleukin 2 receptor, alpha (IL2RA)
26,93	plasminogen activator, urokinase receptor (PLAUR), transcript variant 1
26,75	major histocompatibility complex, class I, E (HLA-E)
23,59	major histocompatibility complex, class II, DM alpha (HLA-DMA)
21,76	leukotriene B4 receptor (LTB4R)
21,06	intercellular adhesion molecule 2 (ICAM2)
20,57	CD37 molecule (CD37), transcript variant 2
20,18	CASP8 and FADD-like apoptosis regulator (CFLAR), transcript variant 1
18,05	major histocompatibility complex, class II, DP alpha 1 (HLA-DPA1), transcript variant 2
16,31	major histocompatibility complex, class II, DM alpha (HLA-DMA)
14,26	CD63 molecule (CD63), transcript variant 1
13,95	caveolin 2 (CAV2), transcript variant 1
13,92	prostaglandin D2 synthase 21kDa (brain) (PTGDS)
13,31	CD74 molecule, major histocompatibility complex, class II invariant chain
12,02	sialic acid binding Ig-like lectin 14 (SIGLEC14)
11,98	CD244 molecule, natural killer cell receptor 2B4 (CD244), transcript variant
11,17	major histocompatibility complex, class I, F (HLA-F), transcript variant 2
Higher in RT monocytes	
Fold-change	**Gene**
1128,92	chemokine (C-C motif) ligand 4-like 1 (CCL4L1)
659,61	chemokine (C-X-C motif) ligand 1 (melanoma growth stimulating activity, alpha) (CXCL1)
481,94	chemokine (C-X-C motif) ligand 2 (CXCL2)
394,81	interleukin 8 (IL8)
206,72	Janus kinase 1 (JAK1)
187,58	tumor necrosis factor receptor superfamily, member 10b (TNFRSF10B), transcript variant 1,
168,28	transforming growth factor, beta receptor II (70/80kDa) (TGFBR2), transcript variant 1,
112,25	interleukin 1, beta (IL1B)
97,50	tumor necrosis factor, alpha-induced protein 3 (TNFAIP3)
88,65	jun proto-oncogene (JUN)
88,23	reactive oxygen species modulator 1 (ROMO1)
52,32	high mobility group box 1 (HMGB1)
52,29	CD164 molecule, sialomucin (CD164)

50,38	interferon regulatory factor 2 binding protein 2 (IRF2BP2) transcript variant 1
47,98	CD58 molecule (CD58), transcript variant 1
Fold-change	**Gene**
44,99	Fc fragment of IgG, low affinity IIa, receptor (CD32) (FCGR2A), transcript variant 1,
37,62	CD44 molecule (Indian blood group) (CD44)
35,50	notch 1 (NOTCH1)
35,32	myeloid differentiation primary response 88 (MYD88), transcript variant 5,
34,57	lipopolysaccharide-induced TNF factor (LITAF), transcript variant 1
34,00	toll-like receptor 2 (TLR2)
29,17	C-type lectin domain family 10, member A (CLEC10A), transcript variant 2
27,35	CD9 molecule (CD9)
25,50	cyclin-dependent kinase inhibitor 2C (p18, inhibits CDK4) (CDKN2C), transcript variant 1
24,37	CD40 molecule, TNF receptor superfamily member 5 (CD40), transcript variant 2
24,13	cyclin-dependent kinase 13 (CDK13)
23,87	platelet/endothelial cell adhesion molecule 1 (PECAM1)
20,63	integrin, alpha L (antigen CD11A (p180),
16,45	prostaglandin E receptor 2 (subtype EP2), 53kDa (PTGER2)
12,78	Homo sapiens signal transducer and activator of transcription 3 (STAT3), transcript variant 1
12,01	CD46 molecule, complement regulatory protein (CD46)
11,31	chemokine (C-C motif) receptor 1 (CCR1)
11,26	tumor necrosis factor (TNF)
10,06	heat shock 105kDa/110kDa protein 1 (HSPH1)
10,05	CD69 molecule (CD69)

Manuscript Number: HEP-15-1041

Supplementary Table 3:

Comparison reverse transmigrating vs. subendothelial CD14+CD16++ monocytes	
Higher in SE monocytes	
Fold-change	**Gene**
40,84	CD63 molecule (CD63), transcript variant 1
23,24	interleukin 2 receptor, gamma (IL2RG)
22,95	D247 molecule (CD247), transcript variant 1
11,82	colony stimulating factor 1 receptor (CSF1R)
Higher in RT monocytes	
Fold-change	**Gene**
122,01	chemokine (C-C motif) ligand 3 (CCL3)
79,40	chemokine (C-C motif) ligand 4-like 1 (CCL4L1)
72,62	interleukin 1, beta (IL1B
53,91	interleukin 8 (IL8)
39,10	chemokine (C-X-C motif) ligand 2 (CXCL2)
31,11	chemokine (C-X-C motif) ligand 1 (melanoma growth stimulating activity, alpha) (CXCL1)
22,69	chemokine (C-C motif) ligand 3 (CCL3)
19,58	tumor necrosis factor, alpha-induced protein 3 (TNFAIP3)
18,45	tumor necrosis factor, alpha-induced protein 8 (TNFAIP8), transcript variant 1
14,10	cyclin D1 (CCND1)
11,97	1 receptor antagonist (IL1RN)
11,33	complement component 5a receptor 1 (C5AR1)
10,07	interleukin 10 (IL10)